

Selective imaging of 3D director fields and study of defects in biaxial smectic A liquid crystals

I.I. Smalyukh¹, R. Pratibha², N.V. Madhusudana², and O.D. Lavrentovich^{1,a}

¹ Chemical Physics Interdisciplinary Program and Liquid Crystal Institute, Kent State University, Kent, OH44242, USA

² Raman Research Institute, 560080 Bangalore, India

Received 16 October 2003 / Received in final form 11 October 2004

Published online 22 February 2005 – © EDP Sciences, Società Italiana di Fisica, Springer-Verlag 2005

Abstract. We report on the selective imaging of different director fields in a biaxial smectic A (SmA_b) liquid crystal using Fluorescence Confocal Polarizing Microscopy (FCPM) and Polarizing Microscopy (PM). The patterns of two directors, namely the director \hat{n}_a perpendicular to the lamellae and the director \hat{n}_b in their planes are visualized by doping the liquid crystal with two fluorescent dyes with different orientation of the transition dipoles with respect to the lamellar matrix. The properties of defects such as disclinations and focal conic domains (FCDs) are consistent with the non-polar D_{2h} -symmetry of the SmA_b mesophase in the studied mixture of bent-core and rod-like molecules: (1) majority of defects in the director \hat{n}_b are half-integer “ $\pm 1/2$ ” disclinations; (2) the integer-strength “ ± 1 ” defects tend to split into the “ $\pm 1/2$ ” disclinations. We compare the vertical cross-sections of the “ ± 1 ” disclinations in the \hat{n}_b field in SmA_b and uniaxial nematic samples. In SmA_b, the “ ± 1 ” disclinations do not escape into the third dimension, while in the nematic samples with Schlieren textures they do despite the surface anchoring at the plates; the experimentally determined director field around the escaped disclination capped by a pair of surface point defects – boojums matches the one predicted recently [C. Chiccoli et al., Phys. Rev. E **66**, 030701 (2002)]. The FCD structure in SmA_b is similar to that in SmA and SmC in terms of the normal to the layers but differs significantly in terms of the director field \hat{n}_b parallel to the smectic layers. The FCDs in SmA_b can be associated with topologically non-trivial configurations of \hat{n}_b in the surrounding matrix that are equivalent to the disclination lines.

PACS. 61.30.-v Liquid crystals – 87.64.Tt Confocal microscopy – 61.30.Jf Defects in liquid crystals – 61.30.Eb Experimental determinations of smectic, nematic, cholesteric, and other structures

1 Introduction

Smectic liquid crystals are formed by 1D stacks of molecular layers [1,2]. The most studied is a uniaxial smectic A (SmA) with the symmetry $D_{\infty h}$, associated with a non-polar arrangement of rod-like molecules perpendicular to the layers. The local optical axis is simultaneously the molecular director $\hat{n}_a \equiv -\hat{n}_a$ and the normal to the layers. Each layer is a 2D fluid. If the rod-like molecules are tilted with respect to the layer normal, an optically biaxial phase of smectic C (SmC) with the local symmetry C_{2h} arises; the tilt creates a vector-like field $\hat{c} \neq -\hat{c}$ (the projection of molecular axes onto the smectic planes) in the plane of each layer [1,2]. During the last decade, the studies of smectic liquid crystals have been revitalized by the introduction of bent-core molecules, also known as bow-shaped and banana-like. One of the interesting directions is the search for the optically biaxial orthogonal non-polar smectic A phase, SmA_b, also called the McMillan phase SmC_M, as suggested by de Gennes [1].

In the simplest case, the orthogonal SmA_b would be composed of box-like molecules with all three axes being orientationally ordered and with a periodic density modulation along one of the directors, say, \hat{n}_a . The symmetry of SmA_b, D_{2h} , is lower than that of SmA, as there is an orientational order in the plane of each layer, but higher than that of SmC, as the molecules are not tilted; the in-plane orientational order is described by a director, $\hat{n}_b \equiv -\hat{n}_b$. Such a structure has been first reported for a liquid crystalline polymer by Leube and Finkelmann [3]. Its physical properties, in particular, prevalence of energetically less costly “ $\pm 1/2$ ” disclinations over non-escaped “ ± 1 ” disclinations has been discussed by Brand et al. [4,5]. The first observation of SmA_b phase in low-molecular thermotropic materials has been reported for a mixture of bent-core (BC) and rod-like (R) molecules by Pratibha, Madhusudana, and Sadashiva [6]. SmA_b was also reported in the mixture of a metallomesogen and 2, 4, 7-Trinitrofluorenone by Hegmann et al. [7] and in the compound with molecules that have covalently connected BC and R parts, by Yelamaggad et al. [8]. Some of the nonlinear bent core compounds synthesized by Dingemans and

^a e-mail: odl@lci.kent.edu

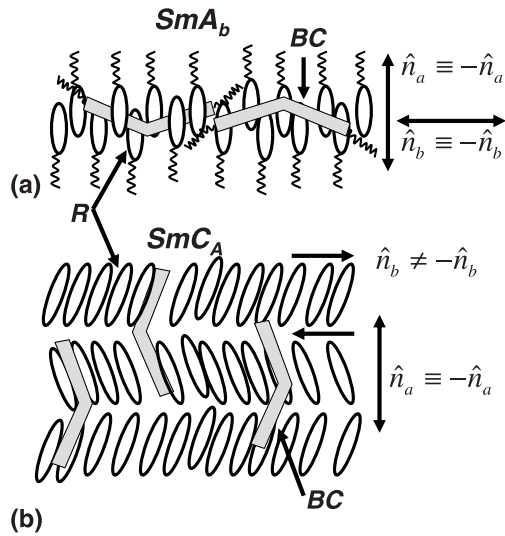


Fig. 1. Orientation of BC and R molecules and the directors in the biaxial smectic of SmA_b type (a) and of SmC_A type (b).

Samulski [9] and Yelamaggad et al. [8] can exhibit the orthogonal biaxial SmA_b and also the biaxial nematic phase.

In the BC-R mixtures, according to the model [6], Figure 1a, the R molecules form a uniaxial SmA matrix with the director $\hat{n}_a \equiv -\hat{n}_a$ perpendicular to the layers, in which the “guest” BC molecules can experience an alignment transition, thus giving rise to a director $\hat{n}_b \equiv -\hat{n}_b$ in the plane of the layers, Figure 1a. Such a model is by no means trivial or obvious, as it has been known for some time that the bent-core type molecules, namely, the cis-isomers of azobenzene derivatives can segregate between the smectic layers, preserving the uniaxial state of the uniaxial SmA host [10]. And indeed, recent computer simulations by Colorado group [11] on a mixture of R and BC molecules found no evidence of the biaxial SmA_b phase; instead, one observes either an anticlinic SmC_A, in which the molecules are tilted within each layer with the direction of tilt alternating from layer to layer, Figure 1b, or a uniaxial SmA with BC molecules in the interlamellae pockets, as in the nanosegregation effect described for trans-to-cis isomerization of an azobenzene derivative in a SmA host [10]. Structures similar to the anticlinic SmC_A rather than to SmA_b have been also reported for systems containing BC molecules by Eremin et al. [12] and Gorecka et al. [13]. In the BC-R mixtures the BC molecules can adopt different orientations with respect to the R molecules and the smectic layers depending on their concentration [6,14], moreover, the orientation of BC molecules within the smectic layers can be also altered by temperature as shown in the recent works by Zhu et al. [14].

The basic difference between SmA_b and SmC_A is that the in-plane direction of orientational order satisfies the condition $\hat{n}_b \equiv -\hat{n}_b$ in the first case and does not satisfy it in the second case, Figure 1a, b. The point symmetry of SmC_A is C_{2v} . Therefore, one might expect a difference in the structure of defects, in particular, in the strength m of disclinations with axes perpendicular to the smectic

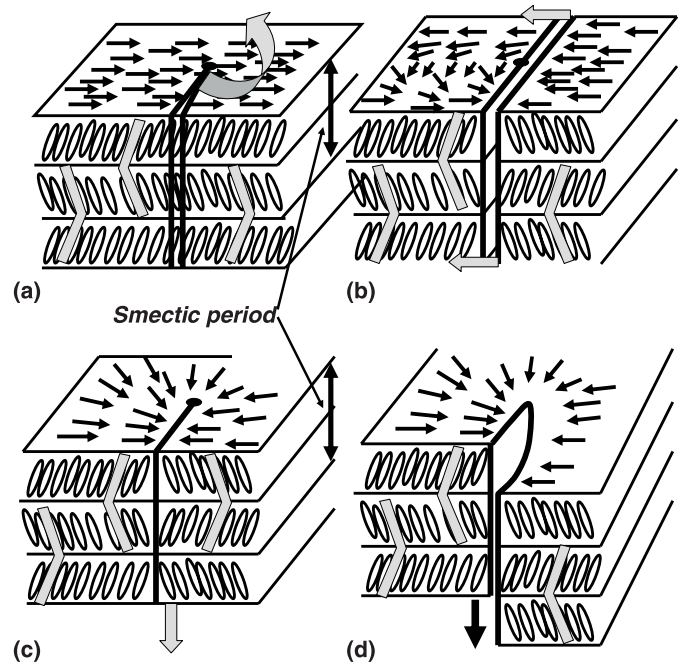


Fig. 2. Formation of a dispiration in SmC_A phase: the originally uniform in-plane vector field in the flat stack of layers (a) is continuously deformed (b) to form the $m = 1/2$ disclination and a wall defect (c) which then relaxes to the dispiration, a combination of the $m = 1/2$ disclination and a screw dislocation (d).

layers; m is defined as the number of revolutions by 2π that the vector (or director) field makes around the defect core when one circumnavigates the core once [2]. Both integer and half-integer m 's are allowed in SmA_b while only integer m 's are topologically allowed in SmC_A. However, as discussed by Takanishi et al. [15] and by Weissflog et al. [16], the half-integer disclinations can still be observed in phases with $\hat{n}_b \neq -\hat{n}_b$ such as SmC_A, in which the tilt *alternates* from layer to layer, when these disclinations pair up with screw dislocations of a small (one, three, etc. lamellae half-periods) Burgers vector, i.e., when they appear as dispirations [17], Figure 2. The reason is that in SmC_A two operations, namely, translation along the layer normal by a half a smectic period and rotation by π restore the original structure, Figure 2. To distinguish SmA_b from SmC_A phase based on the textures only is difficult as the half-integer disclinations in SmA_b and dispirations in SmC_A have similar appearance under the optical microscope. Some of the single-compound materials that were originally reported to exhibit SmA_b phase on the basis of texture observations [18] were later proven to show the polar version of the biaxial smectic phase, SmC_A [19]. On the other hand, the evidence for SmA_b phase in the BC-R mixture [6] is consistent with X-ray and polarized infrared spectroscopy data [20].

In this work, we study the characteristic defects in SmA_b phase of the BC-R mixture, namely, disclinations and focal conic domains, by regular polarizing microscopy and fluorescence confocal polarizing microscopy

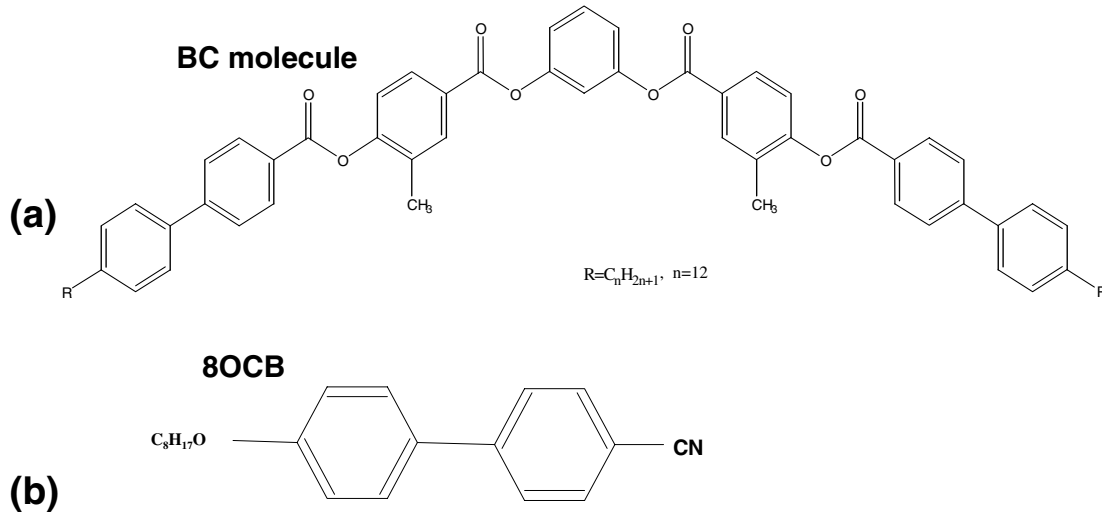


Fig. 3. Molecular structures of the liquid crystal compounds of the BC-R mixture: BC12 (a), 8OCB (b).

(FCPM) [21–24]. We observe splitting of the disclinations of integer strength to the half-integer disclinations in agreement with the orthorhombic non-polar biaxial symmetry of the SmA_b phase. FCPM allows us to resolve the features along the direction of observation (vertical axis \hat{z}) and also to separately visualize the orientational order of two director fields: the one along the layer normal and the one in the plane of the lamellae. We present the “side” views of disclinations in smectic and nematic samples of finite thickness. The experimentally determined director pattern in the nematic samples matches closely the one predicted very recently by a model that takes into account the surface anchoring effects [25]. In the smectic case, the core does not escape, as expected. Furthermore, we explore the focal conic domains (FCDs) in SmA_b and demonstrate that they differ from their counterparts in both SmA [2,26] and SmC [27–29], as they can be associated with the distorted field \hat{n}_b in the surrounding matrix that is equivalent to the field of the disclination lines.

2 Experiment

We study the binary mixtures of 4-octyloxy-4'-cyanobiphenyl (8OCB, Fig. 3b) with rod-like molecules and 1,3-phenylene-bis [4-(3-methylbenzoyloxy)]-4'-n-dodecylbiphenyl-4'carboxylate (BC12, Fig. 3a) with bent-core molecules. The mixture with 89 mole % of 8OCB and 11 mole % of BC molecules exhibits the following phase sequence when cooling from the isotropic phase (IP): IP 85 °C Nematic 57.8 °C SmA 40.3 °C SmA_b [20]. The mixture with 87 mole % of 8OCB and 13 mole % of BC compound exhibits the same phase sequence but the transitions are observed at somewhat higher temperatures: IP 87 °C Nematic 54 °C SmA 48 °C SmA_b [20]. 8OCB is known to have a partial bilayer structure in SmA [30]. X-ray experiments have shown that in the studied 8OCB-BC mixture the rod-like molecules also form a partial bilayer structure and that the BC molecules align within the layers as shown in Figure 1a [20].

In SmA_b , the three symmetry axes are mutually perpendicular and the tensor of dielectric susceptibility has a diagonal form in the frame formed by these axes, with the three principal values being different, $\epsilon_x \neq \epsilon_y \neq \epsilon_z$. The system is optically biaxial, with two optical axes being in the plane perpendicular to the plane of the molecules; each makes an angle $\xi = \arctan \sqrt{\frac{\epsilon_z(\epsilon_y - \epsilon_x)}{\epsilon_x(\epsilon_z - \epsilon_y)}}$ with \hat{n}_a . In a homeotropic texture with $\hat{n}_a \parallel \hat{z}$, under a regular PM, one would observe a dark brush of extinction each time the director \hat{n}_b is parallel to the polarizer or analyzer [31,32]. This degeneracy can be lifted by an insertion of a birefringent plate such as a quartz wedge [2]. One expects ξ to be small (weak biaxiality) as the number of BC molecules that cause the in-plane order and biaxiality in SmA_b is small. Note that optically both SmA_b and SmC_A have similar properties.

SmA_b should exhibit dielectric behavior as all the directors (including the in-plane director $\hat{n}_b = -\hat{n}_b$) are non-polar, in contrast to the materials with polar in-plane axis $\hat{n}_b \neq -\hat{n}_b$ that show an antiferroelectric switching [12,19]. We verified that the studied 8OCB-BC mixture in the SmA_b phase does not exhibit antiferroelectric switching, in agreement with previous studies [6,20]. In addition, the measured average dielectric permittivity below and above the SmA - SmA_b transition differ by less than 10%, which is in contrast to the case of polar biaxial smectic [12].

In the studies of defects, the liquid crystal is sandwiched between two glass plates. The one that is closer to the objective in the FCPM experiment is thin (0.17 mm) to minimize spherical aberrations during the confocal imaging [21,23]. For planar alignment of the director \hat{n}_a we use rubbed polyimide PI2555 (HD MicroSystems). For homeotropic alignment of \hat{n}_a , the plates are spin-coated with the polymer JALS214 (Japan Synthetic Rubber Inc.). In these cells there is no preferred direction for the in-plane \hat{n}_b director and in a regular PM one observes Schlieren textures determined by the distortions of \hat{n}_b .

The two most important features of FCPM imaging of LCs [21,22] are as follows: (a) The LC sample is

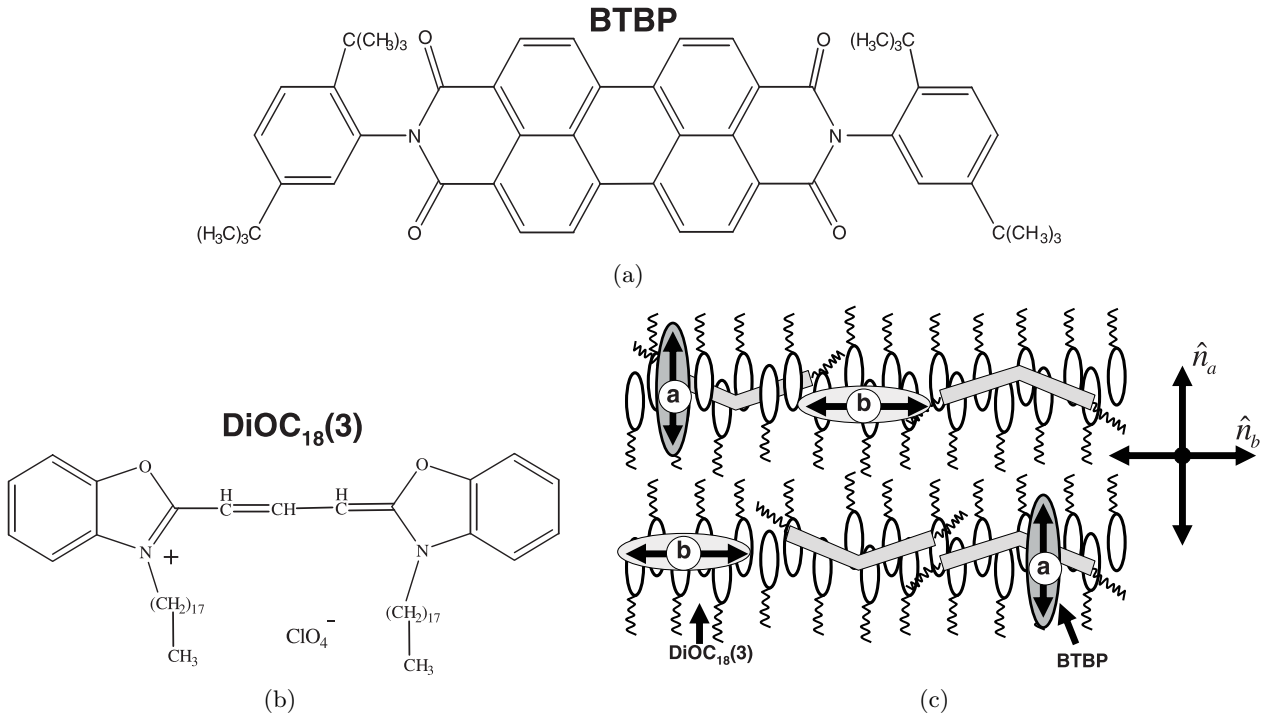


Fig. 4. Molecular structures of the fluorescent dyes BTBP (a) and DiOC₁₈(3) (b) that were used to probe the director structures and their orientation with respect to the directors in SmA_b (c). The mutually orthogonal black double arrows in (c) show the directors \hat{n}_a and \hat{n}_b .

doped with an anisotropic dye, which is aligned by the host, (b) the bulk of the sample is scanned with a focused polarized (usually linearly) laser beam. The probing beam causes fluorescence of the dye molecules; the intensity of fluorescence depends on the dye orientation with respect to the polarization of light. In this work, to distinguish between the two directors, \hat{n}_a and \hat{n}_b , we use two different dyes: *n,n'*-bis(2,5-di-*tert*-butylphenyl)-3,4,9,10-perylenedicarboximide (BTBP, Sigma-Aldrich, Fig. 4a) [21] and 3,3'-dioctadecyloxycarbocyanine perchlorate (DiOC₁₈(3), Molecular Probes, Fig. 4b). In both cases the concentration is only 0.01 weight % and is too small to affect the LC structure or temperatures of phase transitions.

We used a modified Olympus Fluoview BX-50 confocal microscope in the epi-illumination mode with the very same polarizing element \hat{P} setting the polarization directions of excitation and detected fluorescence light, $\hat{P} \parallel \hat{P}_e \parallel \hat{P}_f$. The dye molecules are excited using Ar-laser ($\lambda = 488$ nm) and the fluorescence signal is detected in the spectral range 510–600 nm.

We use the 40X dry objective of numerical aperture $NA = 0.6$. The light depolarization due to this relatively small-aperture objective is negligible and has no significant effect on the FCPM imaging. The power of the used Ar-laser excitation light is less than 1 mW to avoid light-induced reorientation in the dye-doped LC [33]. Only one dye is present in the given sample and thus only one director field is studied at a time. The focused beam scans the sample in the horizontal plane, at a prefixed depth along \hat{z} . Scanning at different depths results in

a three-dimensional pattern of the detected fluorescence light intensity that is related to the angle between the transition dipole of the dye molecules and the polarization of light [21–23]. As shown in the next section, BTBP probes \hat{n}_a and DiOC₁₈(3) probes \hat{n}_b .

3 Results and discussion

3.1 Dye alignment in SmA_b biaxial host and selective imaging of directors

In BTBP, Figure 4a, both absorption and emission transition dipoles are along the long molecular axis [34]. In order to verify that this long axis is aligned along the \hat{n}_a director, we measured the absorption spectra of the 8OCB-BC mixture doped with 0.1% of BTBP in polarized light. Since the 8OCB-BC mixture is transparent in the visible spectral range, the measured absorption is attributed to the dye molecules. The LC is filled into a cell with planar boundary conditions for the \hat{n}_a -director. The absorbance spectra are measured for a small well-aligned area of the sample through the 20 μm pinhole using the Nikon MicroSpectroPhotometry System. The maximum absorbance is registered when the polarizer is parallel to the director \hat{n}_a and minimum for orthogonal orientation, the ratio being $A_{\parallel}/A_{\perp} \approx 2.3$, where A_{\parallel} corresponds to $\hat{P} \parallel \hat{n}_a$ and A_{\perp} corresponds to $\hat{P} \perp \hat{n}_a$. The result shows that the transition dipole of BTBP molecules is along \hat{n}_a , Figure 4c.

The DiOC₁₈(3) molecule has an elongated aromatic core and two aliphatic tails which extend in the direction normal to the core, Figure 4b. Both absorbance and emission dipoles of the DiOC₁₈(3) dye are along the aromatic core [35]. For a planar cell with \hat{n}_a in the plane of cell, the absorbance is stronger for $\hat{P} \perp \hat{n}_a$ than for $\hat{P} \parallel \hat{n}_a$, $A_{\parallel}/A_{\perp} \approx 0.63$, which indicates that the transition dipole is in the plane of the lamellae. We also characterized homeotropic samples with \hat{n}_a perpendicular to the glass plates, using a pinhole to select a homogeneously aligned portion of the texture. The maximum light absorption is observed when the polarizer is along \hat{n}_b , so that DiOC₁₈(3) molecules can serve as the fluorescent probe of the director \hat{n}_b , Figure 4c.

In the FCPM studies, when both the absorption and emission transition dipoles are aligned along the director \hat{n}_i (where $i = a, b$), the efficiency of both absorption and fluorescence can be assumed to be proportional to $(\hat{n}_i \cdot \hat{P})^2$, see reference [22] for a detailed discussion. The intensity of detected fluorescent signal is thus a steep function of the angle β_i between the transition dipole of the dye molecules (and thus the corresponding director) and the polarization \hat{P} of the probing light, $I_i^{\text{FCPM}} \propto I_0 \cos^4 \beta_i$. Confocal mode of the microscope allows one to study the \hat{n}_a and \hat{n}_b directors in both horizontal and vertical planes, with a resolution of about 1 μm . Optical anisotropy of the LC worsens the resolution along the \hat{z} -axis, but typically this complication is not serious for depth of scanning of the order of 10 μm [21–24].

3.2 Structures and defects in the \hat{n}_b director field

Upon cooling down the BC-R mixture with homeotropic SmA texture and \hat{n}_a perpendicular to the glass plates, one obtains Schlieren textures of SmA_b with numerous defects of strength $m = \pm 1$ and $m = \pm 1/2$. In PM textures, Figure 5, the $m = \pm 1$ defects have four dark brushes emanating from the defect center, and the $m = \pm 1/2$ defects have two brushes. In the cells with the substrates treated with JALS214, the ratio of the number of defects is $N_{\pm 1}/N_{\pm 1/2} \approx 1/4$ for the 11%BC+89%8OCB mixture and $N_{\pm 1}/N_{\pm 1/2} \approx 1/5$ for the 13%BC+87%8OCB mixture when calculated right after the transition from SmA phase. The number of $m = \pm 1/2$ defects increases and the number of $m = \pm 1$ defects decreases with time if the sample is kept in SmA_b phase, compare parts (a) and (b) in Figure 5; some of the defects annihilate. After one day, most $m = \pm 1$ defects in a cell with the 13%BC+87%8OCB mixture and JALS214 alignment layers disappear, $N_{\pm 1}/N_{\pm 1/2} \approx 1/90$. In contrast, in the cells with untreated clean glass substrates, the majority of observed defects remain in the form of the $m = \pm 1$ disclinations, Figure 6, as was also noted in reference [6]. The reason for stability of the $m = \pm 1$ defects in the latter case might be surface effects such as tilt of the BC molecules, surface absorption of the BC molecules, or simply surface roughness.

In order to avoid the effect of substrates and their treatment, we studied free-standing homeotropic SmA_b films, Figure 5c. We used 10 μm thick copper foil

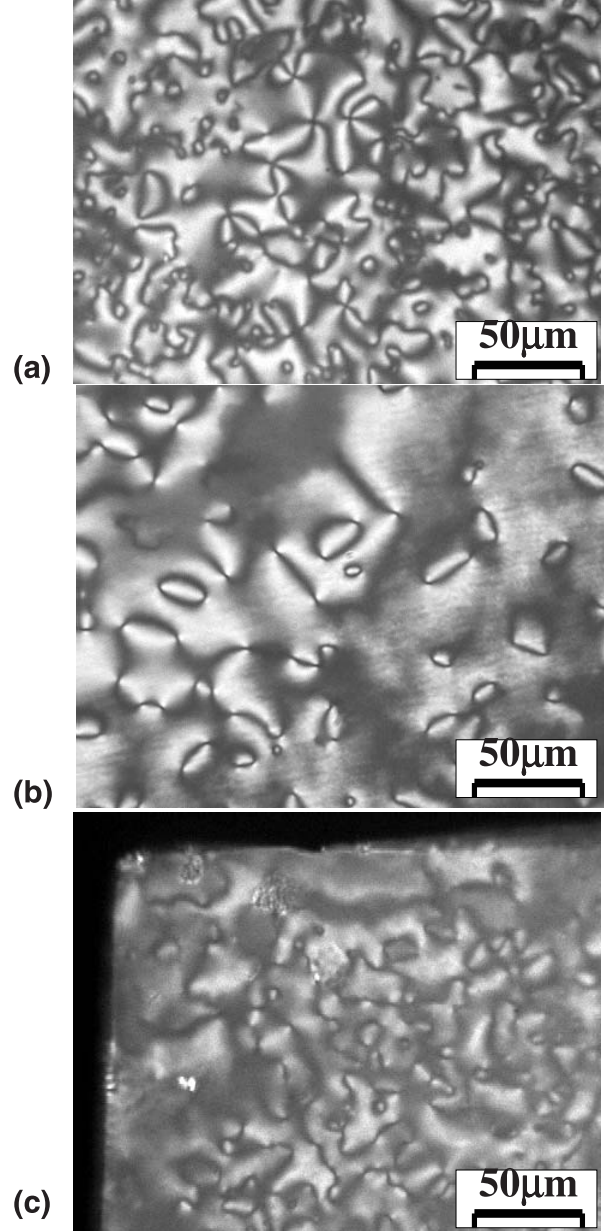


Fig. 5. The Schlieren texture in the BC-R confined sample as observed under the polarizing microscope right after the SmA-SmA_b phase transition (a) and after the sample was kept for about 24 hours in SmA_b phase (b); the Schlieren texture in a free-standing SmA_b film at the corner of a 450 $\mu\text{m} \times 450 \mu\text{m}$ square hole in a 10 μm thick copper foil. The glass substrates in (a, b) were treated with the homeotropic alignment material JALS214. The crossed polarizers in (a–c) are along the edges of images.

with 450 $\mu\text{m} \times 450 \mu\text{m}$ square holes [37, 38]. The films with comparably small variation of thickness $\sim 8 \pm 3 \mu\text{m}$ were drawn in the nematic phase at about 75 $^\circ\text{C}$. With a few exceptions, only half-integer defects were observed. Some of $m = \pm 1$ defects that nucleated at the SmA-SmA_b transition split into the half-integer disclinations. The line defects also slowly annihilated with time.

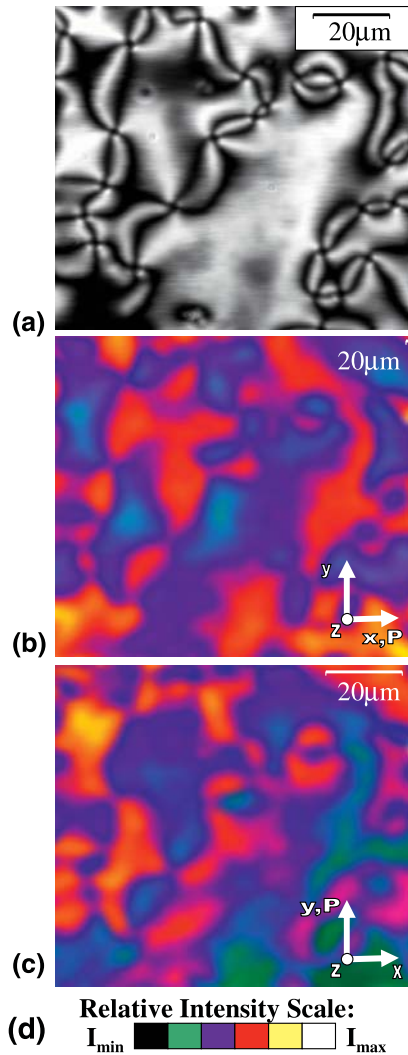


Fig. 6. Spatially co-localized PM (a) and FCPM (b, c) textures of SmA_b sample between two untreated clean glass-substrates. The linear polarization direction in FCPM is marked by “P”. The intensity of fluorescent signal is represented in the color scale (d). The polarizers in (a) are crossed and along the edges of the image.

We now return to the discussion of the textures in cells bounded by two glass plates treated with the JALS214 alignment material. The in-plane FCPM textures, Figures 7a, b, allow one to reconstruct the director field \hat{n}_b and to confirm the existence of both $m = \pm 1$ and $m = \pm 1/2$ centers. In addition, the vertical FCPM cross-sections, Figures 7e, g, reveal that both $m = \pm 1$ and $m = \pm 1/2$ defects have a singular core. The width of the defect cores does not depend on the vertical coordinate \hat{z} , except, perhaps, in the very vicinity of the glass plates, Figures 7e, g. As the image in Figure 7g represents the first FCPM “side-view” of $m = 1$ disclination, it is important to compare it to the corresponding texture of a nematic configuration with $m = 1$, Figure 8. In Figure 8 we used thick ($40 \mu\text{m}$) samples of a uniaxial nematic ZLI-3412 (EM Industries) doped with $\sim 0.01\%$

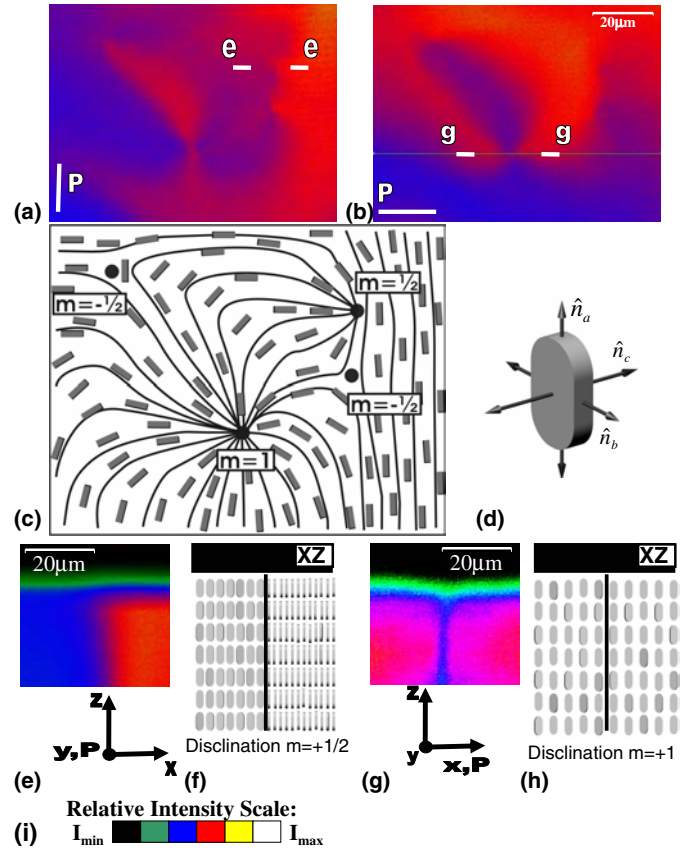


Fig. 7. FCPM textures and director structures corresponding to the defects of different strengths in a SmA_b sample confined between two untreated clean glass-substrates: (a, b) in-plane FCPM textures for two orthogonal polarizations P; (c) in-plane director pattern reconstructed from images (a, b); (d) representation of the directors in the non-polar SmA_b using a plank-like molecule; (e) vertical cross-section of the $m = 1/2$ disclination obtained along the “e-e” line marked in (a) and the corresponding molecular arrangement (f); (g) vertical cross-section of the $m = 1$ disclination obtained along the “g-g” line marked in (b) and corresponding molecular arrangement (h); (i) the relative intensity scale in the FCPM textures. The thin lines in (c) follow the \hat{n}_b -director. The disclinations cores are marked by filled circles in (c) and by the straight lines in (f, h).

the dye BODIPY C_3 (Molecular Probes). The glass plates are spin-coated with polyisoprene [23] for a degenerate tangential orientation of the nematic director \hat{n} .

Comparison of Figures 7g, h and Figure 8 clearly demonstrates the difference in the core structure, as the width of the nematic core increases significantly when one moves away from the glass plates, as the result of the “escape into the third dimension” discovered by Cladis and Kleman [39] and Meyer [40] for cylindrical samples with the defect core along their axes. Note that the actual structure in the sample restricted by two flat plates is very different from the classical structure of director “escape” in the cylindrical samples [39,40] as the director distortions depend strongly on the vertical coordinate \hat{z} and are capped by two point defects – boojums at the plates [25].

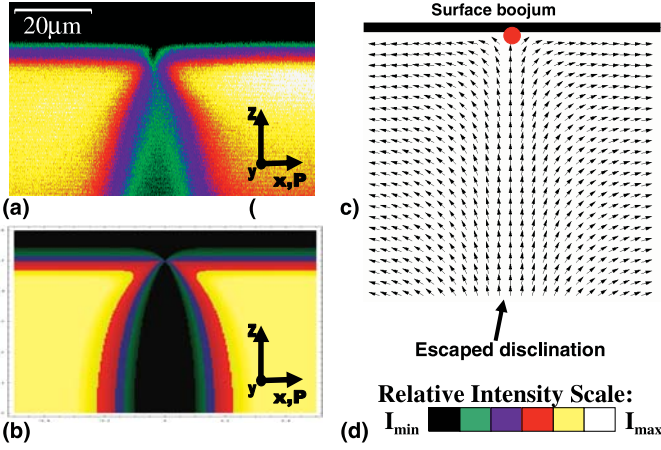


Fig. 8. Core of the “+1” defect in a nematic LC: experimental (a) and computer-simulated (b) FCPM textures and director field (c) near the top part of the LC cell. The relative intensity scale used in the textures (a, b) is shown in (d). The parts (b) and (c) have been calculated using equation (1) and parameters $\eta = 0.99$, $a/d = 0.71$. Note that the core of the escaped configuration becomes narrow near the top glass substrate (black regions in parts (a) and (b)): the escaped disclination is capped by a surface point defect – boojum because of the finite anchoring at the bounding plates. The glass substrates are treated with polyisoprene to produce tangentially-degenerate boundary conditions for the director.

Recently proposed analytical model and computer simulations address the issue of how the escaped configuration is modified by the finite surface anchoring at the surfaces perpendicular to the disclination axis [25]. The director field \hat{n} of the “escaped” structure is characterized by the angle $\theta(r, z)$ between the the cell normal \hat{z} and $\hat{n}(r, z)$. According to reference [25],

$$\theta(r, z) = \arctan \frac{\eta dr \exp(r/A)}{(d/2)^2 - z^2}, \quad (1)$$

where d is the cell thickness, the cylindrical \hat{r} , \hat{z} -coordinates are measured from the cell midplane at the axis of the defect, and η is a dimensionless variational parameter. We simulate the director field, Figure 8c, and the corresponding FCPM texture of the vertical cross-section, Figure 8b, for the case of $\hat{P} \parallel \hat{x}$ (taking into account the effect of finite resolution [21,22] and using parameters $\eta = 0.99$, $a/d = 0.71$ [25]). The color-coding used in the simulations is the same as for the experimental FCPM textures, Figure 8d. The computer-simulated and experimental FCPM textures of vertical cross-sections closely match each other (compare parts (a) and (b) in Fig. 8) proving that the $m = 1$ defects in Schlieren textures of the thin nematic samples do escape, form pairs of boojums at the LC-glass interfaces, and that the model [25] describes the \hat{z} -dependence of the director field very well.

In contrast, the smectic case shows the core that does not depend much on the \hat{z} -coordinate suggesting that these disclinations do not escape into the third dimension. The result is natural as the “escape” of the \hat{n}_b would violate equidistance of smectic layers. In the FCPM texture

of Figure 7g, the core is represented by a narrow stripe, ~ 1 micron wide, which is of the order of the radial resolution of FCPM, with the intensity of the fluorescence signal fading at the center. The latter can be caused by a SmA nature of the core (BC molecules are expelled from the core), by expulsion of the dye $\text{DIOC}_{18}(3)$ molecules, by the decrease of the order parameter of the dye molecules, or all of the above.

As the director \hat{n}_b is confined to the plane perpendicular to the disclination axis in the homeotropic cell, $\hat{n}_a = (0, 0, 1)$, one can apply the Frank model [41] to calculate the elastic energy of distortions $\hat{n}_b(x, y)$ per unit length

$$W_b = \pi m^2 K_b \ln \frac{R}{r_{cb}} + W_{cb}, \quad (2)$$

where K_b is the average elastic constant associated with distortions of the \hat{n}_b -director, r_{cb} is the core radius, and W_{cb} is the core energy, that can be estimated as $W_{cb} \sim \pi m^2 K_b$ [2]. Therefore, the disclination $m = \pm 1$ should be expected to split into two $m = \pm 1/2$ defects as the process can reduce the energy by a factor close to two. The textures in Figure 5 suggest that the splitting of $m = \pm 1$ into $m = \pm 1/2$ defects indeed occurs. Stability of some of the $m = \pm 1$ defects especially in the cells with bare glass substrates even after the sample stays in SmA_b phase for days might be explained by surface effects, such as pinning of the defect cores at surface irregularities.

The experimentally observed splitting of $m = \pm 1$ defects to the $m = \pm 1/2$ defects, Figure 5, is consistent with the D_{2h} symmetry of the studied SmA_b and with the molecular arrangements proposed in [6,20]. However, the observation of the $m = \pm 1/2$ disclinations alone can not be an independent phase identification test to discriminate SmA_b and SmC_A , as these lines can also be observed in SmC_A phase when accompanied by the screw dislocations [15].

3.3 Focal conic domains and the \hat{n}_a director configurations

The FCDs are the most common type of defects in lamellar phases that involve large curvatures of the layers. They are present in both SmA and SmA_b phases, as we demonstrate below by visualizing the three-dimensional configurations of the normal to the layers, the director \hat{n}_a .

We use homeotropic samples of thickness $d = (5 - 20) \mu\text{m}$. In the uniaxial SmA phase, one observes isolated toric FCDs and ellipse-hyperbola FCDs of small eccentricity with their circular or elliptical base located in the bulk of the sample, Figure 9a. When temperature is lowered below the SmA - SmA_b transition, the FCDs tend to shrink (about 10–30% of their original sizes in SmA), Figure 9b. The homeotropic dark texture around the FCD changes into the Schlieren texture containing disclinations in the \hat{n}_b field. In some areas of the sample, the so-called fan-shaped texture is also observed, Figure 9a. In these regions the hyperbola defects of the FCDs are mostly in the plane of the LC cell. When the temperature is lowered below

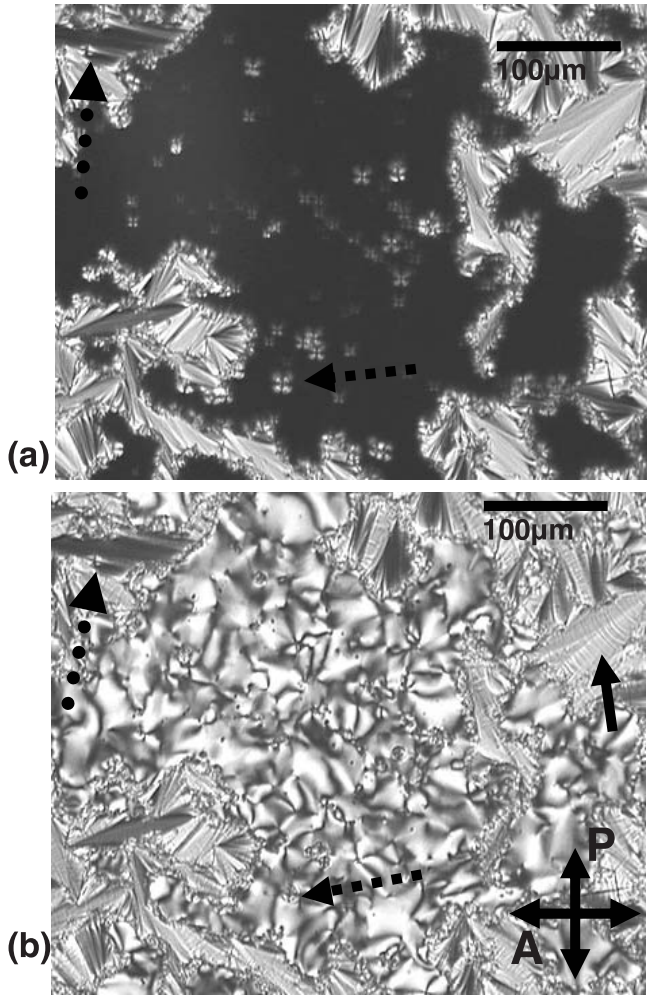


Fig. 9. PM textures obtained in SmA (a) and SmA_b (b) phases of the sample confined between two untreated glass substrates in which both the regions with director $\hat{n}_a \parallel \hat{z}$ and the regions with $\hat{n}_a \perp \hat{z}$ are observed. The double arrows marked by “P” and “A” indicate the orientation of a polarizer and analyzer, respectively. The solid arrow indicates the striations in the fan-shaped parts of the textures. The dotted arrows indicate the FCD with the hyperbola defect in the plane of the cell. The dashed arrow indicates the FCD in a homeotropic part of the sample with the ellipse defect in the plane of cell.

the SmA-SmA_b transition, these regions exhibit striations (marked by a solid arrow in Fig. 9b) that were not present in SmA phase, Figure 9a. Similar striations were observed also in the case of the SmA-SmC phase transition [27,28]. Their appearance may be explained by the layers undulations due to the shrinkage of the layers spacing with decreasing of temperature as well as by distortions and defects in the \hat{n}_b director field, as discussed below.

To determine whether the FCDs preserve their structure at the SmA-SmA_b transition, we study the sample doped with BTBP dye that selectively visualizes \hat{n}_a , Figure 10. As temperature is lowered below the transition to SmA_b phase, no qualitative changes are observed in the FCPM textures. The homeotropic matrix surrounding the FCDs remains dark, as the BTBP transition dipole

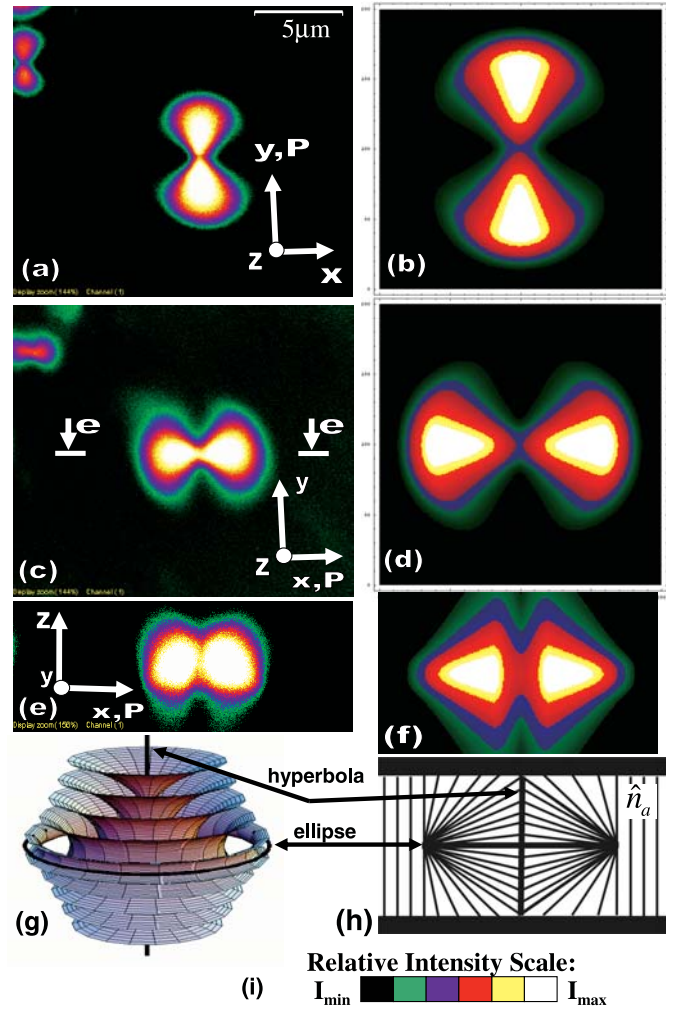


Fig. 10. Experimental (a, c, e), computer-simulated (b, d, f) FCPM textures, the layers pattern (g), and the $\hat{n}_a(x, y = 0, z)$ director field in the vertical cross-section (h) of a focal conic domain in SmA_b. The textures (a) and (c) correspond to the optical sections in the middle plane of the LC cell obtained for different orientations of the polarizer \hat{P} ; vertical cross-section (e) was obtained along the e-e line in (c). The relative intensity scale of the FCPM textures is shown in (i). The sample is confined between two untreated glass substrates.

is perpendicular to the polarization of probing light. The distortions of \hat{n}_a inside the FCDs are similar to those observed in SmA, namely, the director \hat{n}_a is seen to connect all the points of the hyperbola to the points of the ellipse. Figures 10a, c, e show both “horizontal” (parallel to the ellipse) and “vertical” (parallel to the hyperbola) cross-sections of the domain. The eccentricity of ellipse is close to zero, $e \approx 0$; the ellipse is located in the middle plane of the cell. The experimental FCPM textures, Figures 10a, c, e, compare well to the computer-simulated FCPM textures, Figures 10b, d, f, generated using the relationship $I_a^{\text{FCPM}} \propto I_0 \cos^4 \beta_a$, where β_a is the angle between the direction of light polarization \hat{P} and the local \hat{n}_a -director. The reason for some discrepancies seen in the parts (e) and (f) of Figure 10 can be explained by the fact

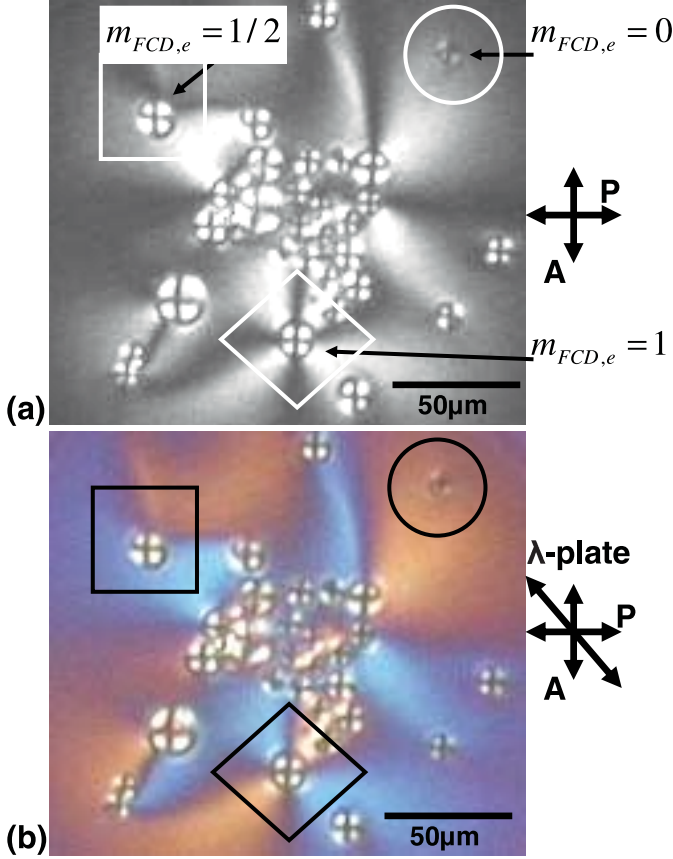


Fig. 11. PM textures of a SmA_b sample under crossed polarizers without (a) and with (b) a 530 nm retardation plate: the FCDs can simultaneously be the curvature defects in the arrangement of smectic layers and the disclinations in the \hat{n}_b director field. The directions of polarizers and the optical axis of the birefringent λ -plate are marked by double arrows. The textures show three different equivalent strengths $m_{\text{FCD},e} = 0$; $+1/2$; and $+1$ of the FCDs as the disclination lines. The easy axis for the \hat{n}_a director at the LC-glass interfaces is along \hat{z} , the normal to the textures (a, b) and the cell substrates. The confining glass substrates were treated with JALS214.

that the difference between the refractive indices for waves polarized along the directors \hat{n}_a and \hat{n}_b is expected to be relatively large, as the material contains 89% of 8OCB with birefringence $\Delta n \sim 0.2$; therefore, it may cause some light defocusing and the apparent asymmetry of the experimental texture (Fig. 10e) with respect to the middle plane of the cell.

Despite the fact that the layered structure of the FCDs in SmA_b phase is similar to that in SmA phase, the appearance of the \hat{n}_b director in the plane of the layers makes the overall structure different. It has long been known that the FCDs in SmC are very different from those in SmA : a disclination in the vector-like field $\hat{c} \neq -\hat{c}$ appears joining the hyperbolae to the two points at the ellipse [27–29]. This disclination makes it possible for the flat SmC layers surrounding the FCD to remain free of defects in the $\hat{c} \neq -\hat{c}$ field. PM observations with two crossed polarizers, Figure 11, and with a quartz wedge inserted between the

sample and the analyzer with the fast direction making an angle $\pi/4$ with the polarizer, Figure 11, demonstrate that FCDs in SmA_b are different from FCDs in both SmA and SmC .

In Figure 11 one observes a cluster of toric FCDs embedded in the flat stack of smectic layers with a uniform $\hat{n}_a \parallel \hat{z}$ and distorted \hat{n}_b that forms a Schlieren texture. The birefringence of the Schlieren texture (exterior of the FCDs) is rather weak as it is related to the difference of the refractive indices $\Delta n_b \sim \sqrt{\varepsilon_x} - \sqrt{\varepsilon_y} \sim 0.01$ [6,36] in the plane of the layers. In contrast, the interior of FCDs is bright which is associated with a large birefringence of the material in the plane that contains the director \hat{n}_a , $\Delta n_a \sim \sqrt{\varepsilon_z} - \sqrt{\varepsilon_x} \sim 0.1$, Figure 11a. The interior of each FCD exhibits four brushes of extinction, which is compatible with the axial symmetry of the \hat{n}_a director configuration, Figures 10g, h. We observe three different types of the exterior texture around the FCDs in SmA_b phase: (a) no brushes at all (the FCD marked by a circle in Fig. 11b); (b) two brushes (FCD inside the square); and (c) four brushes (inside the diamond). The far-field of the \hat{n}_b configuration around the FCDs is thus equivalent to (a) a uniform configuration, $m_{\text{FCD},e} = 0$; (b) a disclination $m_{\text{FCD},e} = 1/2$; and (c) a disclination $m_{\text{FCD},e} = 1$, respectively. The subscript indicates the topological charge that is created by the FCD in the “exterior” matrix of flat layers. The corresponding \hat{n}_b configurations are shown in Figures 12, 13, and 14, respectively, and discussed below for the case of the toric FCDs. In the case of $m_{\text{FCD},e} = 1$, both radial, Figure 14a, and circular, Figure 14b, configurations of \hat{n}_b are observed. We did not observe FCDs with a negative $m_{\text{FCD},e}$, although the textures might contain disclinations with a negative m that compensate the positive charges $m_{\text{FCD},e} = 1/2$ and $m_{\text{FCD},e} = 1$ of the FCDs.

In a toric FCD, there are two types of curved layers inside the cylinder that separates the interior curved layers from the exterior flat layers [2], Figures 12–14. Type I: the curved layers within a distance $r < a$ from the circular defect of radius a are smooth and have no singular points in terms of the normal \hat{n}_a . These layers are topologically equivalent to a half-torus (the part with a negative Gaussian curvature). Type II: The layers at the distance $r \geq a$ from the circular defect have singular points (cusps) at the straight line. In SmA the straight line becomes invisible at sufficiently large distances from the base of the FCD as the cusps become smoother and eventually vanish far away from the FCD’s base; therefore, for $r \gg a$ the type II layers closely resemble flat surfaces.

The SmA - SmA_b transition leads to the appearance of the director $\hat{n}_b \equiv -\hat{n}_b$ field in the plane of the layers. As any direction of \hat{n}_b is possible in the plane of the homeotropic sample, the phase transition causes appearance of defects; some of these defects might be provoked by irregularities at the sample boundaries. The defects might be trapped inside the FCDs. The topological charge of \hat{n}_b configuration in each of the type II layers is equal to the quantity $m_{\text{FCD},e}$ introduced above as the experimentally observed topological charge created by the FCD

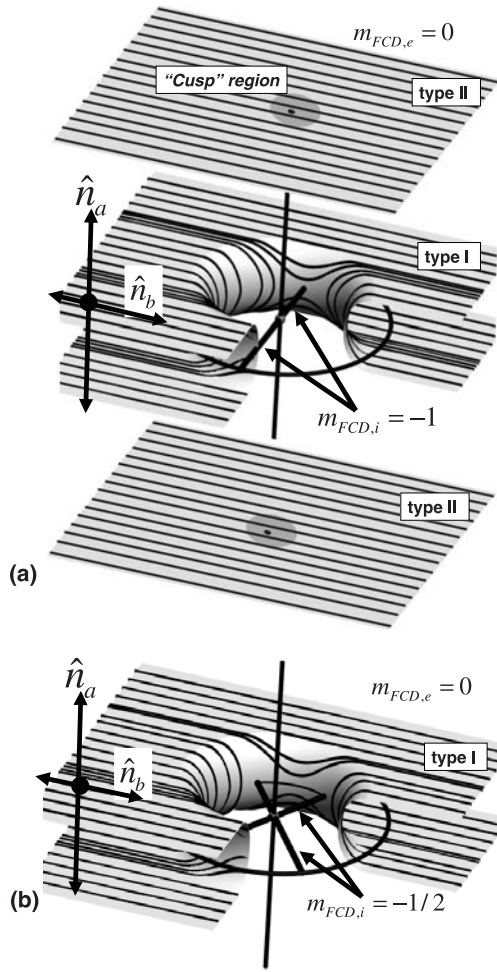


Fig. 12. Configuration of the in-plane director field $\hat{n}_b(x, y, z)$ at the type I and type II layers for a FCD when the \hat{n}_b -director is uniform at large distances from the domain, $m_{\text{FCD},e} = 0$: the two additional disclination lines of strengths $m = -1$ connect the ellipse and the hyperbola (a); they can split into four disclinations of strengths $m = -1/2$ each (b). Only type I layers are shown in (b). The thick lines correspond to the hyperbola (degenerated into a straight line), ellipse (degenerated into a circle), as well as the additional disclination in $\hat{n}_b(x, y, z)$ within the FCD. The $\hat{n}_b(x, y, z)$ -field is represented by the thin lines.

in the surrounding matrix of flat layers. Obviously, the topological properties of \hat{n}_b at the type II layers should be related to those at the type I layers, for there should be no wall defects between the two types of layers; some configurations of \hat{n}_b require topological defects within the type I layers and some do not.

Consider a type II layer far away from the FCD's base with a defect-free \hat{n}_b field, $m_{\text{FCD},e} = 0$, and project this \hat{n}_b field onto the type-I layer beneath the type II layer, Figure 12a. Clearly, the projection creates two defects of the strength $m_{\text{FCD},i} = -1$ each with the layer of the type I, Figure 12a, or four defects of strength $m_{\text{FCD},i} = -1/2$ each, Figure 12b. This construction is similar to the one used to illustrate the Morse theorem in differential geometry, see, for example, reference [42].

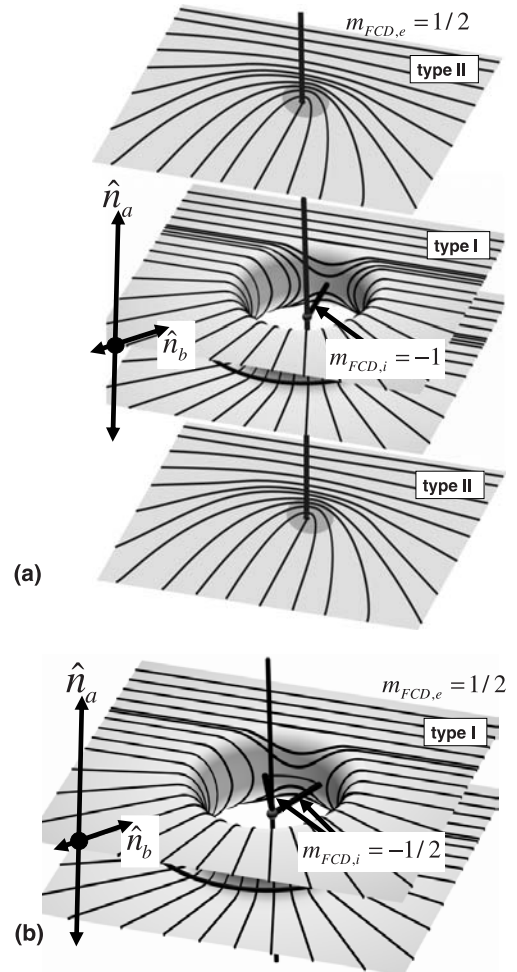


Fig. 13. Configuration of the in-plane director field $\hat{n}_b(x, y, z)$ at the type I and type II layers for a FCD when it is associated with a disclination of strength $m_{\text{FCD},e} = 1/2$: (a) the additional defect line $m = -1$ connects the ellipse and the hyperbola; (b) the $m = -1$ disclination can split into two $m = -1/2$ defect lines.

In a similar way, projection of the director field with $m_{\text{FCD},e} = 1/2$ at the cusp of the layer II onto the layer I creates a defect with $m_{\text{FCD},i} = -1$, Figure 13, and the director field with $m_{\text{FCD},e} = 1$ leads to a defect-free configuration with $m_{\text{FCD},i} = 0$, Figure 14. In general, the topological charge (strength) of the defect within the type II layer is related to the total charge of the defects at the type-I layer as

$$m_{\text{FCD},e} = \frac{1}{2} \sum m_{\text{FCD},i} + 1. \quad (3)$$

If the type II layer contains a defect, the most plausible location of this defect is at the cusp.

The consideration above generalizes from the two layers to the whole set of layers; the relationship becomes the relationship between the strength of a disclination associated with the central line defect formed by all the cusps at the type-II layers (such an association is dictated by energetical reasons; topologically, the defect can be shifted from the central line), and the strength of disclinations

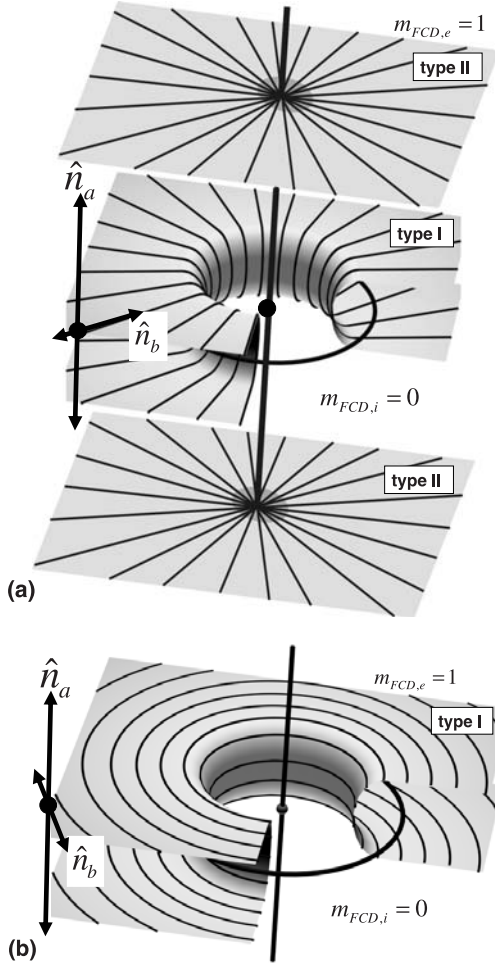


Fig. 14. Configuration of the in-plane director field $\hat{n}_b(x, y, z)$ at the type I and type II layers for a FCD when it is associated with a disclination of strength $m_{\text{FCD},e} = 1$: (a) radial structure of the \hat{n}_b director far from the domain or (b) concentric \hat{n}_b -field far from the domain.

that connect the circular defect to the central line defect. The relationship explains why the FCD with a negative $m_{\text{FCD},e}$ are never observed: their existence would require a large “interior” topological charge, for example, $\sum m_{\text{FCD},i} = -4$ if $m_{\text{FCD},e} = -1$. Note that the disclinations and the respective distortions in the \hat{n}_b field inside of the FCDs are not visible in Figures 9 and 11 because (1) the difference between the refractive indices in the plane of the layers $\Delta n_b \sim \sqrt{\varepsilon_x} - \sqrt{\varepsilon_y} \sim 0.01$ [6,36] is small as compared to the birefringence of the material in the plane that contains \hat{n}_a , $\Delta n_a \sim \sqrt{\varepsilon_z} - \sqrt{\varepsilon_x} \sim 0.1$; (2) the FCDs are too small to resolve the interior features. Nevertheless, the textures presented in Figure 11 clearly indicate that the FCDs in SmA_b can be topologically equivalent to the disclinations of different strength in the \hat{n}_b -field outside the domains.

One of the situations described above is actually a well-known result for FCDs in a regular SmC , in which Perez et al. [27] observed two defect lines each of strength $m_{\text{FCD},i} = -1$ joining the circle and the central line, in this case $m_{\text{FCD},e} = 0$. The situation with $m_{\text{FCD},e} = 1$

and $m_{\text{FCD},i} = 0$ has been already envisioned [27–29] but never observed, while the situation $m_{\text{FCD},e} = 1/2$ and $m_{\text{FCD},i} = -1$ has been never mentioned before.

We also would like to stress that the overall conservation law for the topological charges in the Schlieren texture in general involves only $m_{\text{FCD},e}$ values; for a circular film with a fixed director orientation at the periphery (e.g., \hat{n}_b normal to the bounding circle in the freely-suspended film),

$$\sum m_{\text{FCD},e} + \sum m = 1,$$

where m 's are the topological charges of vertical wedge disclinations in the system of flat layers outside any FCDs. Using the experimental textures and following the brushes of extinction associated with the FCDs with $m_{\text{FCD},e} > 0$, we establish that the positive strength of these FCDs is compensated by negative-strength disclinations $m < 0$ in the Schlieren texture.

Note that since the local structure of SmA_b is of point symmetry D_{2h} , the defects with integer $m_{\text{FCD},e}$ and $m_{\text{FCD},i}$ can split into pairs of half-integer defects, Figures 12b, 13b. In yet another case (not shown), only one of the “ -1 ” disclinations inside of the FCD could split into two “ $-1/2$ ” defects but the other one can remain non-split. In this case, three additional defect lines are present in the plane of ellipse. In SmC , only integer-strength disclinations can be observed [27–29]. The situation is expected to be more complicated in SmC_A , as the half-integer defects inside of the FCDs would require addition of screw dislocations. Certainly, configurations with integer lines shown in Figures 12a, 14a, and 14b are all possible in the SmC_A phase. The configurations with half-integer lines such as presented in Figures 12b, 13a, and 13b can also be observed in the SmC_A phase if the disclinations are accompanied with the screw dislocations.

So far we analyzed only the situations when the elliptical bases of the defects are located in the LC bulk. When the ellipse is at the boundary of SmA_b sample, the additional defect lines within the FCD can be present or not, depending on the orientation of easy axis for the \hat{n}_b -director at the interface, surface anchoring strength, as well as the $\hat{n}_b(x, y, z)$ -field far from the domain, Figure 15.

4 Conclusions

We demonstrated the selective 3D imaging of the two mutually orthogonal director fields in biaxial lamellar LCs using the Fluorescence Confocal Polarizing Microscopy. These director patterns were visualized by doping the liquid crystal with two fluorescent dyes that exhibit different orientations of the transition dipoles with respect to the lamellar matrix. The selective imaging of different directors with FCPM might be useful in studies of other biaxial mesophases with different symmetry that were recently discovered and theoretically predicted in the pure compounds and mixtures [4–9,11–16,43–46]. The FCPM and polarizing microscopy observations revealed the basic

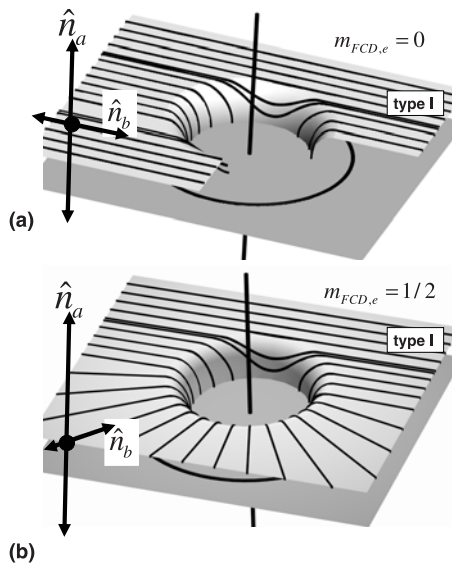


Fig. 15. The FCDs with (a) $m_{\text{FCD},e} = 0$ and (b) $m_{\text{FCD},e} = 1/2$ with their elliptical bases at the LC-glass interface: the defects in addition to the ellipse and hyperbola can arise or not, depending on surface anchoring, easy axis for the \hat{n}_b -director at the LC-glass interface, and the $\hat{n}_b(x, y, z)$ director field in the bulk far from the domains.

features of disclinations and focal conic domains in the nonpolar biaxial smectic SmA_b .

The majority of defects in the director \hat{n}_b (in the plane of SmA_b lamellae) are half-integer disclinations. The integer-strength defects that nucleate at $\text{SmA} - \text{SmA}_b$ transition tend to split into the “ $\pm 1/2$ ” disclinations. In SmA_b phase, the “ ± 1 ” disclinations do not escape into the third dimension. This is in contrast to the nematic samples with Schlieren textures where the “ ± 1 ”-defects do escape despite the surface anchoring at the confining substrates; the director field around the escaped disclination is capped by a pair of surface point defects – boojums. The experimentally reconstructed director field in the vertical cross-section of the escaped configuration closely follows the result theoretically predicted in [25]. Both half-integer and integer-strength disclinations in SmA_b phase have singular cores.

The focal conic domains in SmA_b have the layers structure similar to that in other smectic phases such as SmA and SmC . However, the associated configurations of the in-plane director \hat{n}_b are very different from that observed for FCDs in SmC . Namely, the FCDs in SmA_b can be associated with a topologically non-trivial configuration of \hat{n}_b in the surrounding matrix. In other words, the FCDs in SmA_b might have a hybrid character being defects in layers configuration and, simultaneously, defects in \hat{n}_b . We observed FCDs that are equivalent to the defects of strengths “+1” and “+1/2” in the outside matrix of the director \hat{n}_b ; these topological charges are cancelled by vertical wedge disclinations of opposite charge located nearby.

The properties of defects are consistent with the non-polar D_{2h} -symmetry of SmA_b mesophase in the studied mixture of BC and R molecules in which the imaginary “arrows” of the bow-shaped BC molecules are parallel to

the R-molecules and to the normal to the SmA_b layers. However, as numerous recent studies suggest [12–14, 20], a different orientation with the “arrows” being in the planes of smectic layers is also possible giving rise, for example, to the SmC_A phase. We expect the structural features of the defects in the SmC_A phase to be similar to these in SmA_b phase, in terms of singular core of the “ ± 1 ” disclinations and FCD structures (including their associations with the non-trivial $m_{\text{FCD},e} \neq 0$). It is the structure of the “ $\pm 1/2$ ” defect lines that would be different in SmA_b and SmC_A as in the later case the disclinations must be accompanied by the screw dislocations. To verify the presence of the screw dislocations associated with the disclinations, one would need to resort to the scale of observations that is much smaller than the spatial resolution limits of optical microscopy (e.g., freeze structure and electron microscopy) as the Burgers vector of these dislocations might be as small as one half of the SmC_A period.

The work was partially supported by donors of the Petroleum Research Fund, administered by the American Chemical Society, grant 35306-AC7 and the National Science Foundation, Grant DMR-0315523. We thank Prof. B.K. Sadashiva for the BC compound. We thank D. Allender, A. Jakli, M. Kleman, Yu.A. Nastishin, M. Nobili, B.I. Senyuk, and S.V. Shiyonovskii for helpful discussions. We also thank the referees of European Physical Journal E for useful suggestions.

References

1. P.G. de Gennes, J. Prost, *The Physics of Liquid Crystals* (Clarendon Press, Oxford, 1993)
2. M. Kleman, O.D. Lavrentovich, *Soft Matter Physics: An Introduction* (Springer-Verlag, New York, 2003)
3. H. Leube, H. Finkelmann, *Makromol. Chem.* **191**, 2707 (1990); **192**, 1317 (1991)
4. H.R. Brand, P.E. Cladis, H. Pleiner, *Macromolecules* **25**, 7223 (1992)
5. H.R. Brand, P.E. Cladis, H. Pleiner, *Eur. Phys. J. B* **6**, 347 (1998)
6. R. Pratibha, N.V. Madhusudana, B.K. Sadashiva, *Science* **228**, 2184 (2000)
7. T. Hegmann, J. Kain, S. Diele, G. Pelzl, C. Tschierske, *Angew. Chem. Int. Ed.* **40**, 887 (2001)
8. C.V. Yelamaggad, S.K. Prasad, G.G. Nair, I.S. Shashikala, D.S. Shankar Rao, C.V. Lobo, S. Chandrasekhar, *Angew. Chem. Int. Ed.* **43**, 3429 (2004)
9. L.A. Madsen, T.J. Dingemans, M. Nakata, E.T. Samulski, *Phys. Rev. Lett.* **92**, 145505 (2004); B.R. Acharya, A. Primak, S. Kumar, *Phys. Rev. Lett.* **92**, 145506 (2004); K.J.K. Semmler, T.J. Dingemans, E.T. Samulski, *Liq. Cryst.* **24**, 799 (1998)
10. Y. Lansac, M.A. Glaser, N.A. Clark, O.D. Lavrentovich, *Nature (London)* **398**, 54 (1999); B. Zalar, O.D. Lavrentovich, H. Zeng, D. Finotello, *Phys. Rev. E* **62**, 2252 (2000)
11. P.K. Maiti, Y. Lansac, M.A. Glaser, N.A. Clark, *Phys. Rev. Lett.* **88**, 065504 (2002)
12. A. Eremin, S. Diele, G. Pelzl, H. Nadasi, W. Weissflog, J. Salfetnikova, H. Kresse, *Phys. Rev. E* **64**, 051707 (2001)

13. E. Gorecka, M. Nakata, J. Mieczkowski, Y. Takanishi, K. Ishikawa, J. Watanabe, H. Takezoe, S.H. Eichhorn, T.M. Swager, *Phys. Rev. Lett.* **85**, 2526 (2000)
14. M.H. Zhu, M.R. Dodge, T. Shioda, C. Rosenblatt, D.D. Parker, J. Kim, M. Neubert, *Liq. Cryst.* **31**, 1381 (2004); M.H. Zhu, C. Rosenblatt, J. Kim, M. Neubert, *Phys. Rev. E* **70**, 031702 (2004)
15. Y. Takanishi, H. Takezoe, A. Fukuda, J. Watanabe, *Phys. Rev. B* **45**, 7684 (1992)
16. W. Weissflog, S. Richter, E. Dietzmann, J. Risse, S. Diele, P. Schiller, G. Pelzl, *Cryst. Res. Technol.* **32**, 271 (1997)
17. W.F. Harris, *Phil. Mag.* **22**, 949 (1970)
18. B.K. Sadashiva, A. Reddy, R. Pratibha, N.V. Madhusudana, *J. Mater. Chem* **12**, 943 (2002)
19. A. Reddy, B.K. Sadashiva, *J. Mater. Chem* **14**, 310 (2004)
20. R. Pratibha, N.V. Madhusudana, B.K. Sadashiva, *Phys. Rev. E* **71**, 011701 (2005)
21. I.I. Smalyukh, S.V. Shiyankovskii, O.D. Lavrentovich, *Chem. Phys. Lett.* **336**, 88 (2001)
22. S.V. Shiyankovskii, I.I. Smalyukh, O.D. Lavrentovich, in *Defects in Liquid Crystals: Computer Simulations, Theory and Experiments*, edited by O.D. Lavrentovich, P. Pasini, G. Zannoni, S. Zumer, NATO Science Series, Vol. 43 (Kluwer Academic Publishers, the Netherlands, 2001), p. 229
23. I.I. Smalyukh, O.D. Lavrentovich, *Phys. Rev. Lett.* **90**, 085503 (2003)
24. I.I. Smalyukh, O.D. Lavrentovich, *Phys. Rev. E* **66**, 051703 (2002)
25. C. Chiccoli, I. Feruli, O.D. Lavrentovich, P. Pasini, S.V. Shiyankovskii, C. Zanoni, *Phys. Rev. E* **66**, 030701(R) (2002)
26. M. Kleman, *Points, Lines, and Walls in Liquid Crystals, Magnetic Systems, and various ordered media* (Wiley, Chichester, 1983)
27. A. Perez, M. Brunet, O. Parodi, *J. Phys. Lett. France* **39**, 353 (1978)
28. L. Bourdon, J. Sommeria, M. Kleman, *J. Phys. France* **43**, 77 (1982)
29. Y. Bouligand, M. Kleman, *J. Phys. France* **40**, 79 (1979)
30. A.J. Leadbetter, R.M. Richardson, C.N. Colling, *J. Phys. Colloq. France* **36**, C1-37 (1975); A.J. Leadbetter, J.C. Frost, J.P. Gaughan, G.W. Gray, A. Mosley, *J. Phys. France* **40**, 375 (1979)
31. P. Pieranski, P. Oswald, *Les Cristaux Liquides*, Tome 2 (GB Science Publishers, France, 2002), p. 688
32. R.E. Stoiber, S.A. Morse, *Crystal identification with the polarizing microscope* (Chapman & Hall, New York, 1994); A.F. Konstantinova, B.N. Grechushnikov, B.V. Bokut, E.G. Balyashko, *Optical properties of crystals*, in Russian (Nauka i Tehnika, Minsk, 1995), p. 94
33. I. Janossy, *Phys. Rev. E.* **49**, 2957 (1994)
34. A.J. Bur, S.C. Roth, S.C. Thomas, *Rev. Sci. Instr.* **71**, 1516 (2000)
35. J. Yguerabide, L. Stryer, *Proc. Nat. Acad. Sci. USA* **68**, 1217 (1971)
36. R. Pratibha, N.V. Madhusudana, B.K. Sadashiva, *Mol. Cryst. Liq. Cryst.* **365**, 755 (2001)
37. V. Nazarenko, A. Nych, *Phys. Rev. E* **60**, R3495 (1999)
38. Yu.A. Nastishin, M. Kleman, J. Malthete, H.T. Nguyen, *Eur. Phys. J. E* **5**, 353 (2001)
39. P.E. Cladis, M. Kleman, *J. Phys. France* **40**, 325 (1979)
40. R.B. Meyer, *Phil. Mag.* **27**, 405 (1973)
41. F.C. Frank, *Disc. Farad. Soc.* **25**, 1 (1958)
42. B.A. Dubrovin, A.T. Fomenko, S.P. Novikov, *Modern Geometry – Methods and applications* (Springer, New York, 1992); D. Hilbert, S. Cohn-Vossen, *Geometry and the Imagination* (Chelsea Publishing Company, New York, 1952)
43. D.R. Link, G. Natale, R. Shao, J.E. McLennan, N.A. Clark, E. Korblova, D.M. Walba, *Science* **278**, 1924 (1997)
44. M.W. Schroder, S. Diele, N. Pancenko, W. Weissflog, G. Pelzl, *J. Materials* **12**, 1331 (2002)
45. M.Y. Huang, A.M. Pedreira, O.G. Martins, A.M. Figueiredo Neto, A. Jakli, *Phys. Rev. E* **66**, 031708 (2002)
46. T.C. Lubensky, L. Radzihovsky, *Phys. Rev. E* **66**, 031704 (2002)